Available online at www.sciencedirect.com
SCIENCE DIRECT®
Journal of Power Sources 119–121 (2003) 278–284
JOURNAL OF POWER SOURCES
www.elsevier.com/locate/jpowsour

A comparative structural and electrochemical study of monoclinic $Li_3Fe_2(PO_4)_3$ and $Li_3V_2(PO_4)_3$

Sébastien Patoux[a], Călin Wurm[a], Mathieu Morcrette[a], Gwenaëlle Rousse[b], Christian Masquelier[a,*]

[a]*Laboratoire de Réactivité et de Chimie des Solides, CNRS UMR 6007, Université de Picardie Jules Verne, 33 rue Saint-Leu, 80039 Amiens Cedex, France*
[b]*Institut Laue Langevin, BP 156, F-38042 Grenoble Cedex 9, France*

Abstract

Pure monoclinic $Li_3M_2(PO_4)_3$ (M: Fe, V) powders (<1 μm in diameter) were obtained by an original route that involved initial homogenization of precursors in aqueous solution followed by slow evaporation and annealing under controlled atmosphere at moderate temperatures. The crystal structure of $Li_3V_2(PO_4)_3$ was determined for the first time through Rietveld refinements of neutron diffraction data. As for $Li_3Fe_2(PO_4)_3$, Li is distributed within three crystallographic sites, fully occupied at room temperature. The values of the temperature factors on Li(2) and Li(3) sites (five-fold coordination) were found significantly higher than that of Li(1) (four-fold coordination). $Li_3V_2(PO_4)_3$ shows four reversible redox phenomena upon insertion of two Li^+ (V^{3+}/V^{2+} couple), at 1.98, 1.88, 1.73 and 1.70 V vs. Li. By comparison, $Li_3Fe_2(PO_4)_3$ shows two reversible redox phenomena upon insertion of two Li^+ (Fe^{3+}/Fe^{2+} couple), at 2.88 and 2.73 V vs. Li. Experimental capacities close to the theoretical ones were obtained after optimal composite electrode preparation through ball-milling. In situ X-ray diffraction showed very minor changes from $Li_3M_2(PO_4)_3$ to $Li_5M_2(PO_4)_3$. Additionally, Li is extracted from $Li_3V_2(PO_4)_3$ towards $V_2(PO_4)_3$ (V^{4+}/V^{3+} and V^{5+}/V^{4+} couples) through four redox phenomena at 3.59, 3.67, 4.06 and 4.35 V vs. Li. Despite all these phase transitions, the $[M_2(PO_4)_3]$ framework is remarkably stable on cycling, particularly for M: Fe, while partial vanadium dissolution into the electrolyte occurs either on deep reduction to 1.5 V or deep oxidation to 4.6 V vs. Li.

Keywords: Structural study; Monoclinic; Crystallographic

1. Introduction

Recently, polyanion 3-D structures built of PO_4 tetrahedra and FeO_6 octahedra have engendered much interest for their potential use as cheap positive electrodes for lithium rechargeable batteries [1]. Efforts towards this relatively novel class of intercalation hosts for lithium have focused on systems such as the olivine $Li_{1-x}FePO_4$ [2,3] and NASICON compositions $Li_xFe_2(SO_4)_3$ [4] or $Li_{3+x}Fe_2(PO_4)_3$ [5,6] into which reduction/oxidation of Fe^{3+}/Fe^{2+} occurs at potentials close to 3.43, 3.55 and 2.8 V vs. Li/Li^+, respectively. For applications, the material of choice of the so-called poly-anionic structures is with no doubt the olivine $LiFePO_4$ that, since the pioneering discovery of Padhi et al. [2] has gained much interest [7–9]. Recent optimization of $LiFePO_4$ has focused on: (i) increasing the electronic conductivity of composite electrodes through carbon coating on the active material particles [7,8]; and (ii) lowering the synthesis temperature to ∼400 °C with the use of strongly reactive iron oxalate under N_2 [9]. $LiFePO_4$ stands as a serious candidate for the next generation of Li-based polymer or Li-ion batteries.

Materials of general composition $A_xMM'(PO_4)_3$ (A: Li, Na, . . .; M and M′: transition metal element) adopt either the "A"-form or "B"-form (NASICON) that differ in the 3-D connectivity between $MM'(PO_4)_3$ units. Among this very rich family of compositions and crystal structures, the NASICON $Li_3Fe_2(PO_4)_3$ [5,6], $LiTi_2(PO_4)_3$ [10] and $Li_3V_2(PO_4)_3$ [11,12] were shown to react electrochemically with lithium at 2.8, 2.5 and 3.7 V vs. Li^+/Li, for the $Fe^{3+/2+}$, $Ti^{4+/3+}$ and $V^{3+/4+}$ couples, respectively. Delmas and co-workers were the first to demonstrate nice reversibility through a two-phase process between $LiTi_2(PO_4)_3$ and $Li_3Ti_2(PO_4)_3$ (138 mAh/g) [10] but the practical use of these materials was still under question, due to their low intrinsic electronic conductivity. We recently paid particular attention to circumvent this handicap and reported [13,24] that

* Corresponding author.
E-mail address: christian.masquelier@sc.u-picardie.fr (C. Masquelier).

0378-7753/03/$ – see front matter © 2003 Elsevier Science B.V. All rights reserved.
doi:10.1016/S0378-7753(03)00150-2

energetic ball-milling of Fe(III)-containing phosphates with conductive carbon (carbon SP or acetylene black) resulted in a very significant improvement of their electrochemical performances.

Lithium extraction out of the monoclinic form of $Li_3V_2(PO_4)_3$ (anti-NASICON) has been demonstrated by Barker and Saidi [14] and Sato et al. [15]. More recently, promising behaviour was reported by Saïdi et al. [16] and Nazar et al. [17–19] in the course of our study. Our study aims to compare the electrochemical and structural behaviour of isotypical iron and vanadium phosphates upon lithium insertion and/or extraction. We will show, after a detailed examination of the crystal structures of monoclinic $Li_3Fe_2(PO_4)_3$ and $Li_3V_2(PO_4)_3$ (determined from powder neutron diffraction data) that, despite an impressive number of phase transitions, very minor structural changes occur over a wide range of lithium contents into the $M_2(PO_4)_3$ framework. While Fe(III) can only be reduced to Fe(II) ($Li_{3+x}Fe_2(PO_4)_3$), V(III) can be either oxidized to V(IV) ($Li_{3-x}V_2(PO_4)_3$) or reduced to V(II) ($Li_{3+x}V_2(PO_4)_3$). Similar comparisons were recently reported [20] for $Li_{1\pm x}MP_2O_7$ (M(III) = Fe, V).

2. Experimental

Pure A-$Li_3M_2(PO_4)_3$ (M: Fe, V) powders were obtained by an original route that involved initial homogenization of precursors in aqueous solution (1 mol/l) followed by slow evaporation of H_2O at 100 °C and volatile species at 300 °C under air and further annealing (400–800 °C) of the resulting solid until crystallization. Stoichiometric amounts of $Fe(NO_3)_3{\cdot}9H_2O$ and LiH_2PO_4 were mixed in the case of $Li_3Fe_2(PO_4)_3$. Stoichiometric amounts of NH_4VO_3 (V(V)) and LiH_2PO_4 were mixed in the case of $Li_3V_2(PO_4)_3$. In this case, the annealing was conducted up to 750 °C (12 h) under a gas flow of N_2/H_2 (10%) to achieve reduction of V(V) to V(III). Note that for both compounds, the initial mixing of precursors in solution was essential to favour lower synthesis temperatures that resulted in smaller particle sizes (spherical, less than 1 μm in diameter) than by direct solid state synthesis (particle sizes >50 μm).

The crystal structure of A-$Li_3V_2(PO_4)_3$ was solved from room temperature powder diffraction data recorded on the high resolution neutron powder diffractometer D1A ($\lambda = 1.9104$ Å) at ILL-Grenoble (France). The crystal structure of A-$Li_3Fe_2(PO_4)_3$ was determined from room temperature powder diffraction data recorded on the neutron multicounters powder diffractometer G4.2 ($\lambda = 2.3433$ Å) at LLB of Saclay (France). Both structures were obtained from Rietveld refinements [21] using the program Fullprof [22] from an initial set of atomic coordinates of $Li_3Fe_2(PO_4)_3$ previously determined from single-crystal diffraction data [23]. Differential scanning calorimetry measurements (DSC) were performed on a Mettler DSC 25 device driven by the interface TC11, with a heating rate of 10 K/min.

The electrochemical tests were performed in standard Swagelok™ cells with a lithium foil at the negative electrode and A-$Li_3M_2(PO_4)_3$ (M: Fe, V)/carbon composites at the positive electrode. A Whatman GF/D borosilicate glass fiber sheet saturated with a 1 M $LiPF_6$ electrolyte solution in 1:1 (w/w) of dimethyl carbonate/ethylene carbonate constitutes the separator member. The active material powders were mechanically ball-milled with Super P carbon (SP, MMM Carbon, Belgium) in the proportions 200/40 mg (16.67% of carbon) in a stainless steel container using a SPEX 8000 mixer to generate sufficient impacts/shocks [24]. A MacPile automatic cycling/data recording system (Biologic SA, Claix, France) operating in galvanostatic mode at *C*/10 regime, was used for the electrochemical data recording. For in situ X-ray diffraction, a modified Swagelok-type was mounted, horizontally, on a D8 Bruker diffractometer (Co Kα radiation, θ–θ geometry, PSD counter) and monitored by a MacPile system in a galvanostatic intermittent titration technique (GITT) mode at *C*/20 regime (1 h) with open circuit (1 h) to collect the X-ray data.

3. Results and discussions

3.1. Crystal structures at room temperature

For both $Li_3Fe_2(PO_4)_3$ and $Li_3V_2(PO_4)_3$, lithium ordering at room temperature over three crystallographic sites generates a slight monoclinic distortion [23] that cannot be well spotted by standard X-ray diffraction nor low-resolution neutron diffraction. Complementary synchrotron X-ray diffraction experiments were carried out at LURE (Orsay) to confirm the purity of $Li_3Fe_2(PO_4)_3$ [24] and $Li_3V_2(PO_4)_3$. Similarly to the iron counterpart [23], $Li_3V_2(PO_4)_3$ presents a monoclinic distortion of the classic orthorhombic cell at room temperature (Fig. 1). We confirmed by differential scanning calorimetry and temperature-controlled X-ray diffraction the sequences of α (monoclinic) ↔ β (orthorhombic) ↔ γ (orthorhombic) phase transitions due to lithium disordering between room temperature and 573 K. Note that under air, $Li_3V_2(PO_4)_3$ is not stable above 800 K, at which temperature oxidation of V(III) takes place.

The Rietveld refinements of the neutron diffraction patterns of A-$Li_3Fe_2(PO_4)_3$ and A-$Li_3V_2(PO_4)_3$, recorded at room temperature (α-forms), are presented in Fig. 2. The space group $P2_1/n$ (first setting, binary axis ***c***) was preferred rather than $P2_1/c$ (binary axis ***b***) in order to keep the same setting as that of the original paper of Bykov [23]. A-$Li_3Fe_2(PO_4)_3$ ($a = 8.571(1)$ Å, $b = 12.017(1)$ Å, $c = 8.616(1)$ Å, $\gamma = 90.52(1)^\circ$, $V = 887(1)$ Å^3) and A-$Li_3V_2(PO_4)_3$ ($a = 8.605(1)$ Å, $b = 12.038(1)$ Å, $c = 8.591(1)$ Å, $\gamma = 90.60(1)$ $V = 890(1)$ Å^3) are isostructural with the monoclinic form of $Fe_2(SO_4)_3$ with $Z = 4$ [25]. Satisfactory conventional *R*-factors were obtained $R_{wp} = 3.69\%$ and $R_B = 3.76\%$ for A-$Li_3Fe_2(PO_4)_3$, whereas $R_{wp} = 7.08\%$ and $R_B = 7.97\%$

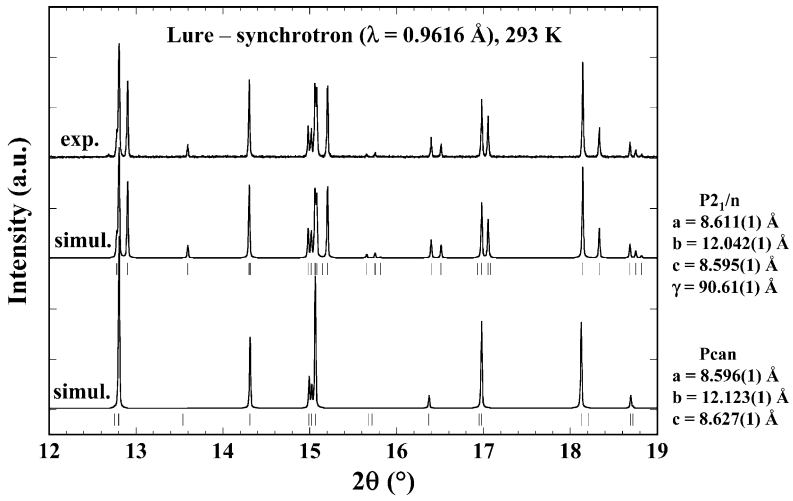

Fig. 1. X-ray diffraction pattern (exp.) of the room temperature form of A-$Li_3V_2(PO_4)_3$ recorded from a synchrotron radiation with $\lambda = 0.9616$ Å. The experimental pattern is compared with two simulated patterns (simul.) calculated in monoclinic $P2_1/n$ or orthorhombic *Pcan* space group.

for A-$Li_3V_2(PO_4)_3$. Hence, less accuracy was obtained for A-$Li_3V_2(PO_4)_3$ as vanadium is essentially transparent to neutron radiation. However, all the bond-strengths and polyhedra distortions for both compounds are in perfect accordance with the formula of Zachariasen [26,27].

All the 20 independent atoms of the unit cell are in general position 4*e* (Table 1). The transition element M (M: Fe or V) is distributed over two independent positions. At room temperature, lithium ions fully occupy three distinct sites, two of them being in five-fold coordination (Li(2) and Li(3)), whereas Li(1) is in four-fold coordination. The peculiar distribution of lithium ions within the framework is worth of consideration as they are located within (***a***, ***c***) ''conduction planes'' (Fig. 3) that generate strong anisotropy in ionic conduction. More interestingly, even is the fact that for both compounds, the refined temperature factors on Li(2) and Li(3) sites (five-fold coordination) are significantly higher than that of Li(1), which indicates that ionic conduction is likely to occur mainly along [0 0 1]. To further support this point, during the order–disorder $\alpha \rightarrow \beta \rightarrow \gamma$ transitions, only the Li(2) and Li(3) sites are involved, their occupancy factors becoming fractionate. As discussed elsewhere [28], these observations are of importance for a good understanding of the complex phase transitions that occur during lithium extraction from $Li_3V_2(PO_4)_3$.

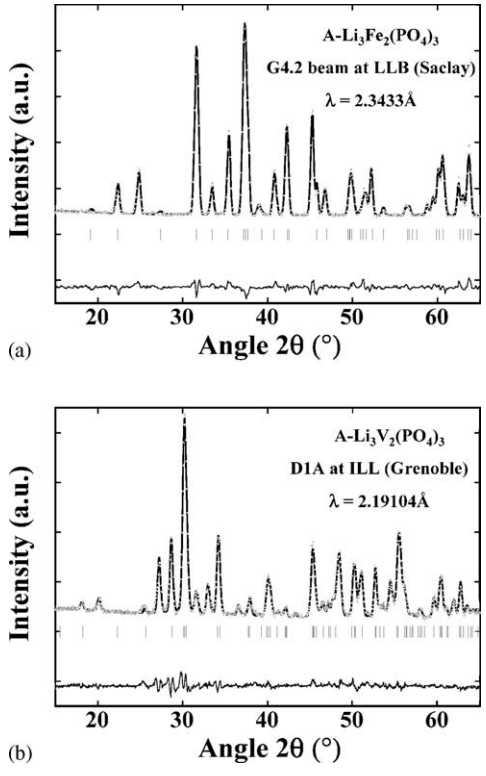

Fig. 2. Neutron diffraction Rietveld profiles of the experimental (circles) and calculated (full lines) patterns for (a) A-$Li_3Fe_2(PO_4)_3$ and (b) A-$Li_3V_2(PO_4)_3$. The vertical lines indicate the possible Bragg positions. Differences between experimental and calculated patterns are also drawn below.

3.2. Insertion of lithium between 3.0 and 1.0 V vs. Li

Lithium insertion is possible into both A-$Li_3M_2(PO_4)_3$ (M: Fe, V) compounds. Experimental galvanostatic and

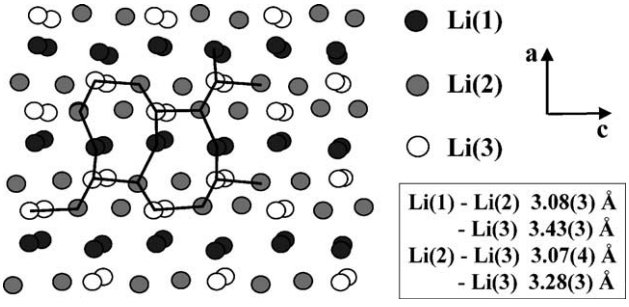

Fig. 3. Projection on the (*a*, *c*) plane of the lithium ions distribution in A-$Li_3M_2(PO_4)_3$ (M: Fe, V). Segments are drawn between neighboring Li positions to indicate possible conduction pathways.

Table 1
Atomic coordinates and isotropic displacement factors obtained by Rietveld refinements of neutron diffraction data for A-$Li_3Fe_2(PO_4)_3$ (normal) and A-$Li_3V_2(PO_4)_3$ (bold)

Atoms	Sites	Wyckoff positions			B_{iso} (Å^2)	Occupancy
M_1 (Fe)	4e	0.2462(5)	0.1079(3)	0.4619(4)	0.26(7)	1
M_1 **(V)**		**0.2461**[a]	**0.1072**[a]	**0.4606**[a]	**0.61**[a]	**1**
M_2 (Fe)	4e	0.7541(2)	0.3950(3)	0.4708(4)	0.22(7)	1
M_2 **(V)**		**0.7534**[a]	**0.3943**[a]	**0.4703**[a]	**0.59**[a]	**1**
P_1	4e	0.1030(9)	0.1484(5)	0.1069(8)	0.9(2)	1
		0.1068(9)	**0.1489(8)**	**0.1014(11)**	**1.4(2)**	**1**
P_2	4e	0.60393(9)	0.3495(6)	0.1160(8)	0.6(1)	1
		0.6004(9)	**0.3493(7)**	**0.1164(11)**	**1.5(2)**	**1**
P_3	4e	0.0359(7)	0.4932(6)	0.2512(11)	1.0(1)	1
		0.0349(9)	**0.4924(7)**	**0.2474(12)**	**1.1(2)**	**1**
O_1	4e	0.4292(7)	0.3309(5)	0.0885(7)	0.9(1)	1
		0.4257(9)	**0.3305(6)**	**0.0915(9)**	**1.5(2)**	**1**
O_2	4e	0.9237(7)	0.1497(5)	0.1151(7)	0.6(1)	1
		0.9262(9)	**0.1471(6)**	**0.1108(10)**	**1.3(2)**	**1**
O_3	4e	0.3527(7)	0.2620(5)	0.4806(7)	0.6(1)	1
		0.3547(8)	**0.2607(6)**	**0.4799(8)**	**1.2(2)**	**1**
O_4	4e	0.8022(7)	0.2193(5)	0.4972(64)	0.3(2)	1
		0.8041(9)	**0.2185(7)**	**0.4952(9)**	**1.5(2)**	**1**
O_5	4e	0.1669(8)	0.0389(5)	0.0580(7)	1.4(1)	1
		0.1727(10)	**0.0394(7)**	**0.0518(8)**	**1.6(2)**	**1**
O_6	4e	0.6455(7)	0.4713(5)	0.0920(7)	0.8(1)	1
		0.6435(9)	**0.4747(6)**	**0.0883(9)**	**1.2(2)**	**1**
O_7	4e	0.4507(7)	0.0689(4)	0.3678(8)	0.4(1)	1
		0.4500(8)	**0.0667(5)**	**0.3688(9)**	**0.9(2)**	**1**
O_8	4e	0.9273(8)	0.4037(5)	0.3132(7)	0.6(1)	1
		0.9277(9)	**0.4033(6)**	**0.3196(9)**	**1.0(2)**	**1**
O_9	4e	0.1709(6)	0.4317(4)	0.1710(7)	0.4(1)	1
		0.1697(9)	**0.4291(6)**	**0.1697(9)**	**1.4(2)**	**1**
O_{10}	4e	0.5979(7)	0.0701(4)	0.1273(8)	0.6(1)	1
		0.6098(9)	**0.0750(6)**	**0.1346(10)**	**1.6(2)**	**1**
O_{11}	4e	0.1635(6)	0.1868(5)	0.2636(7)	0.3(2)	1
		0.1660(9)	**0.1862(7)**	**0.2670(9)**	**1.5(2)**	**1**
O_{12}	4e	0.6374(7)	0.3168(5)	0.2868(8)	1.0(1)	1
		0.6399(9)	**0.3176(6)**	**0.2868(9)**	**1.1(2)**	**1**
Li_1	4e	0.288(2)	0.320(2)	0.275(2)	0.1(4)	1
		0.292(3)	**0.328(2)**	**0.298(2)**	**0.5(4)**	**1**
Li_2	4e	0.571(2)	0.202(2)	0.419(2)	1.4(5)	1
		0.571(3)	**0.195(2)**	**0.421(3)**	**2.9(6)**	**1**
Li_3	4e	0.901(3)	0.243(2)	0.291(3)	5.2(7)	1
		0.911(4)	**0.233(3)**	**0.305(4)**	**4.7(8)**	**1**

[a] Due to the "transparency" of vanadium in neutron diffraction, these parameters must be refined one by one, and cannot be incorporated in the final refinement.

derivative curves are plotted in Fig. 4. Complete lithium insertion leads to compositions close to $Li_5M_2(PO_4)_3$ in which Fe or V are reduced to M(II). Both compounds show, at first sight, similar electrochemical behaviour on reduction with the existence of a well-defined intermediate composition $Li_4M_2(PO_4)_3$. It is remarkable to note that the 1 V difference between the average positions of Fe^{3+}/Fe^{2+} and V^{3+}/V^{2+} redox couples is the same as that observed for these two couples in $Li_{1+x}FeP_2O_7$ and $Li_{1+x}VP_2O_7$ [20] and also the same as that established in aqueous solution.

From PITT measurements, we indicated recently [24] that lithium insertion within the two-phase domains $Li_3Fe_2(PO_4)_3$–$Li_4Fe_2(PO_4)_3$ (2.88 V vs. Li) and $Li_4Fe_2(PO_4)_3$–$Li_5Fe_2(PO_4)_3$ (2.73 V vs. Li) was kinetically limited more by electron or ion transport within each phase rather than from phase front migration. The existence of an intermediate phase $Li_4Fe_2(PO_4)_3$ results probably from lithium insertion into a given new crystallographic site that generates local reduction of the nearest Fe positions. A close examination of the relative positions of MO_6 octahedra within the structure besides the interstitial space available for Li insertion does not favour the M(1) nor the M(2) site to be reduced first between $Li_3Fe_2(PO_4)_3$ and $Li_4Fe_2(PO_4)_3$. Hence, we believe that a new lithium distribution occurs within the interstitial space for $Li_4Fe_2(PO_4)_3$ which does not necessarily generate Fe^{3+}/Fe^{2+} charge ordering. This is supported by the experimental data of Manthiram [29] on lithium insertion into monoclinic $Fe_2(SO_4)_3$: there is, in this case, only one intercalation plateau (at 3.6 V vs. Li) between $Fe_2(SO_4)_3$ and $Li_2Fe_2(SO_4)_3$, even though iron is

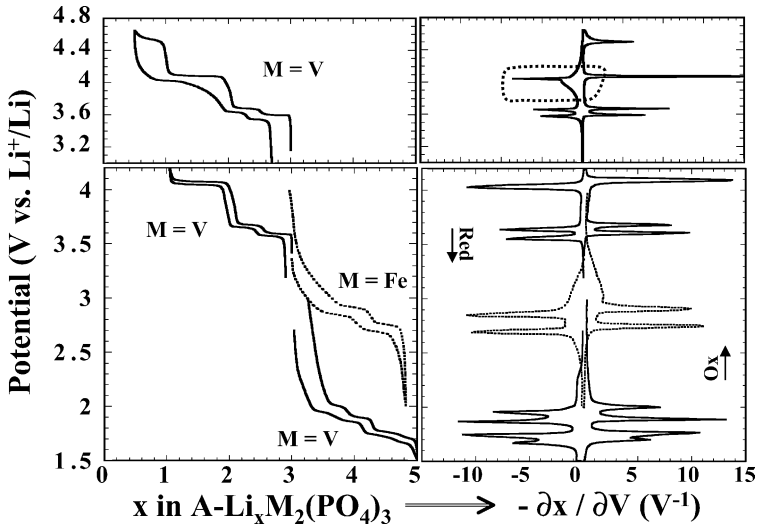

Fig. 4. Left part: charge-discharge and discharge–charge profiles of A-$Li_3Fe_2(PO_4)_3$ and A-$Li_3V_2(PO_4)_3$ recorded under galvanostatic conditions (C/10) in the 1.50–4.65 V range vs. Li^+/Li. Right part: derivative curves of potentiodynamic intermitent titration technique (PITT) data (10 mV steps for $t_{max} = 1$ h, I_{min} equivalent to C/20).

distributed over two distinct crystallographic sites. Despite the phase transition at $x = 1$, optimized electrodes of $Li_{3+x}Fe_2(PO_4)_3$ cycle remarkably well in the potential range 3.5–2.0 V for $0 \leq x \leq 1.8$ (320 Wh/kg for a mean voltage of 2.75 V) as can be seen in Fig. 5. In situ X-ray diffraction experiments [30] confirmed the existence of two two-phase domains and revealed only very minor, and reversible, changes in the framework over a whole discharge/charge cycle.

As for A-$Li_3Fe_2(PO_4)_3$, lithium may be inserted into A-$Li_3V_2(PO_4)_3$ according to, at first sight, a similar mechanism: two main intercalation plateaus at 1.86 and 1.73 V vs. Li are distinguished. More careful experiments than those recently reported by Sato [31] reveal though that there are actually four distinct phenomena at 1.98, 1.86, 1.73 and 1.70 V vs. Li (Fig. 4), each of them corresponding roughly to 0.5 electrons exchanged per formula unit. The theoretical capacity was achieved experimentally, with the complete reduction of the V^{3+} ions into V^{2+} ions. There is however a rapid capacity fade on cycling due to vanadium dissolution into the electrolyte, as already mentioned for $LiVP_2O_7$ [20].

In situ X-ray diffraction (Fig. 5) shows a very similar behaviour for both compositions, the framework being maintained throughout the whole insertion range. As a number of diffraction peaks of the monoclinic $P2_1/n$ unit cell overlap, satisfactory refinement of the lattice parameters of the intermediate composition $Li_4M_2(PO_4)_3$ and of the final composition $Li_5M_2(PO_4)_3$ was difficult. We found however very similar trends for both compounds between the two definite compositions $Li_3M_2(PO_4)_3$ and $Li_4M_2(PO_4)_3$: contraction along [1 0 0] (−1.5%),

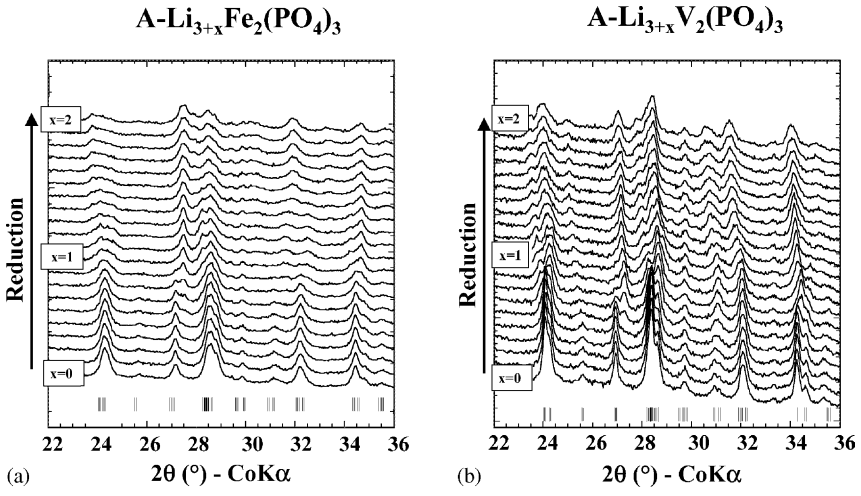

Fig. 5. In situ X-ray diffraction recorded during Li insertion in GITT mode into (a) $Li_3Fe_2(PO_4)_3$ and (b) $Li_3V_2(PO_4)_3$. Diffractometer D8 Bruker, Co Kα, θ–θ geometry, PSD counter.

elongation along [0 1 0] and [0 0 1] (+1.6 and +1.5%, respectively) and increase of the monoclinic distortion to 91.1°. This represents only a minor global volume change and accounts for the nice reversibility of the system.

3.3. Extraction of lithium between 3.0 and 4.65 V vs. Li

In this region of potentials, only $Li_3V_2(PO_4)_3$ is of interest as Fe^{3+} cannot be oxidized to Fe^{4+} below 5 V vs. Li^+/Li. The oxidation of V^{3+} to V^{4+} by lithium extraction out of monoclinic $Li_3V_2(PO_4)_3$ was reported by Nanjundaswamy [32] and Sato [33] and more recently by Barker [14,16] and Nazar [17]. On the other hand, successful attempts to prepare the NASICON form of $Li_3V_2(PO_4)_3$ by ion exchange from the sodium analogue $Na_3V_2(PO_4)_3$ allowed to identify an interesting Li-extraction plateau at 3.77 V vs. Li for the V^{3+}/V^{4+} redox couple [12].

Contrary to Sato et al. [33], we found that there was no need to dope monoclinic $Li_3V_2(PO_4)_3$ with zirconium to get nice reversibility of this material upon oxidation. Only careful electrode preparation (intimate mixing with conductive carbon) is needed to fully oxidize V^{3+} into V^{4+} from the pristine $Li_3V_2(PO_4)_3$ to the Li-extracted $LiV_2(PO_4)_3$ (Fig. 4) which corresponds to an energy density of ∼ 500 Wh/g. Our results are extremely similar to those reported recently [16,17]: three reversible voltage plateaus at 3.59, 3.67 and 4.06 V vs. Li are clearly distinguished, stressing the existence of $Li_{2.5}V_2(PO_4)_3$, $Li_2V_2(PO_4)_3$ and $LiV_2(PO_4)_3$ compositions as intermediate phases. Note that even under *C*/5 charge and discharge rates, very small polarization of the cell was observed. The nature of the intermediate phases has been addressed elsewhere by means of ex situ neutron diffraction [17] or in situ X-ray diffraction [28].

As we mentioned earlier in this paper, the greater mobility of lithium on Li(3) sites (five-fold coordination) probably favors this site to be emptied first during oxidation. If so, from the examination of Li–vanadium nearest environments ($d_{Li(1)–V(1)}$ = 2.95 Å, $d_{Li(2)–V(2)}$ = 2.90 Å, $d_{Li(3)–V(2)}$ = 2.73 Å) this would be associated with oxidation of vanadium on the V(2) site first. In the same way, the very low mobility of lithium on Li(1) sites (four-fold coordination) is a good indication that this site is probably the remaining one occupied at the intermediate composition $LiV_2(PO_4)_3$. Between $Li_3V_2(PO_4)_3$ and $LiV_2(PO_4)_3$, the volume of the monoclinic unit cell was found to decrease from 890 to 824 $Å^3$ as a result of oxidation of V^{3+} to V^{4+}. It is interesting to note then that despite this rather big unit cell contraction ($\Delta V/V = -7.4\%$) the overall $Li_3V_2(PO_4)_3$–$LiV_2(PO_4)_3$ is highly reversible as only 13% of the capacity was lost after 100 cycles at room temperature at *C*/10, between 3.0 and 4.2 V vs. Li (Fig. 6). Additional cycling tests within narrower voltage windows (3.0–3.5 V; first two plateaus, 1 e^- exchanged and 3.9–4.2 V; third plateau, 1 e^- exchanged) lead to a similar stability.

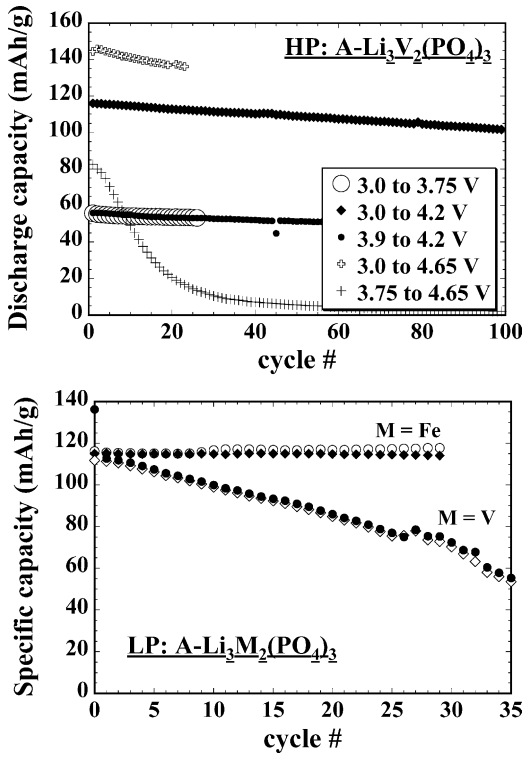

Fig. 6. Evolution of specific capacities under a *C*/10 cycling regime at "high" potential (HP) for A-$Li_3V_2(PO_4)_3$, using different cut-off voltages, and at low potential (LP) for both A-$Li_3Fe_2(PO_4)_3$ and A-$Li_3V_2(PO_4)_3$ (full symbols: on discharge; opened symbols: on charge).

On increasing the upper cut-off voltage to 4.65 V vs. Li, $LiV_2(PO_4)_3$ may be further oxidized to ∼$V_2(PO_4)_3$ which leads to a specific capacity of 197 mAh/g. Fig. 4 shows a dissymmetry between the shapes of the charge and discharge galvanostatic curves. The fourth oxidation peak at 4.35 V (stronger polarization of the cell for this step) presents on discharge a large hysteresis that is hidden within the first broad reduction peak on discharge between 4.0 and 3.8 V. There is no structural irreversibility even on extracting lithium to $V_2(PO_4)_3$ as indicated by: (i) the four plateaus on charge are still observed on extensive cycling; and (ii) in situ X-ray diffraction [28] showed that the pattern of $Li_3V_2(PO_4)_3$ after a full cycle is the same as that of the pristine compound. Fig. 6 shows however a more rapid decay of the capacity on cycling than when the upper voltage cut-off is limited to 4.2 V. As mentioned for $Li_{1-x}VP_2O_7$ [20], progressive dissolution of vanadium in the electrolyte and/or electrolyte decomposition at high voltage may be at the origin of this phenomenon. Note that upon oxidation from $LiV_2(PO_4)_3$ to $V_2(PO_4)_3$, we observed a unit cell expansion from 824 to 835 $Å^3$.

Chemical extraction of lithium (using NO_2BF_4 in acetonitrile for 7 days under stirring) out of monoclinic $Li_3V_2(PO_4)_3$ allowed preparation of $V_2(PO_4)_3$ with no lithium residue (confirmed by chemical analysis). A similar experiment had already been reported by Gopalakrishnan et al. [34] to prepare the NASICON form of $V_2(PO_4)_3$ by

sodium extraction out of $Na_3V_2(PO_4)_3$ (in this case, Cl_2 in $CHCl_3$ was used). The obtained $V_2(PO_4)_3$ was placed in an air-free cell for X-ray diffraction and indexed to a monoclinic unit cell in the same space group ($P2_1/n$) as that of $Li_3V_2(PO_4)_3$. The overall unit cell contraction found is of $\Delta V/V = -6\%$, with the in situ X-ray diffraction data (-6.2%) and in good agreement with the results of Nazar et al. (-6.6%) [17].

4. Conclusion

A-$Li_3V_2(PO_4)_3$ and A-$Li_3Fe_2(PO_4)_3$ are two interesting positive electrode materials for lithium and lithium-ion batteries. In A-$Li_xV_2(PO_4)_3$ ($0 \leq x \leq 5$), we highlighted the presence of eight ($4 + 4$) two-phase domains in the 1.0–4.65 V vs. Li^+/Li range. The $Li_3V_2(PO_4)_3$–$LiV_2(PO_4)_3$ reaction, which corresponds to the exchange of one electron per V and the complete oxidation of V^{3+} into V^{4+}, is nicely reversible with a good capacity retention (∼130 mAh/g) in cycling, at a mean potential of 3.86 V thus giving an energy density of ∼500 Wh/kg. Such a material, with a cheaper transition metal element, could almost approach the performances of $LiCoO_2$. The use of the third electron, conducting to A-$V_2(PO_4)_3$, would increase these numbers, but the cycling behaviour is not optimized yet. A-$Li_3Fe_2(PO_4)_3$, which is only active for lithium insertion, can reversibly exchange two electrons at ∼ 2.75 V vs. Li^+/Li (∼350 Wh/kg) onto two distinct plateaus, both corresponding to the reduction of the Fe^{3+} ions into Fe^{2+} for A-$Li_5Fe_2(PO_4)_3$.

Acknowledgements

The authors are grateful to Juan Rodriguez-Carvajal for the neutron diffraction data collecting at LLB Saclay and Erik Elkaim and J.-P. Lauriat for the synchrotron measurements at Lure, Orsay. J.-M. Tarascon is gratefully acknowledged for his support in the project and his critical review of the manuscript.

References

[1] J.B. Goodenough, A.K. Padhi, K.S. Nanjundaswamy, C. Masquelier, US Patent, 5,910,382 (1999).
[2] A.K. Padhi, K.S. Nanjundaswamy, J.B. Goodenough, J. Electrochem. Soc. 144 (4) (1997) 1188–1194.
[3] A.K. Padhi, K.S. Nanjundaswamy, C. Masquelier, S. Okada, J.B. Goodenough, J. Electrochem. Soc. 144 (5) (1997) 1609–1613.
[4] S. Okada, K.S. Nanjundaswamy, A. Manthiram, J.B. Goodenough, in: Proceedings of the 36th Power Sources Conference, 6–9 June 1994.
[5] A.K. Padhi, K.S. Nanjundaswamy, C. Masquelier, J.B. Goodenough, J. Electrochem. Soc. 144 (8) (1997) 2581–2586.
[6] C. Masquelier, A.K. Padhi, K.S. Nanjundaswamy, J.B. Goodenough, J. Solid State Chem. 135 (1998) 228–234.
[7] N. Ravet, J.B. Goodenough, S. Besner, M. Simoneau, P. Hovington, M. Armand, in: Proceedings of the 196th Meeting of the Electrochemical Society, Hawai, October 1999 (Abstract 127).
[8] H. Huang, S.C. Yin, L.F. Nazar, Electrochem. Solid State Lett. 4 (10) (2001) A170–A172.
[9] A. Yamada, S.C. Chung, K. Hinokure, J. Electrochem. Soc. 148 (3) (2001) A224–A229.
[10] C. Delmas, F. Cherkaoui, A. Nadiri, P. Hagenmuller, Mater. Res. Bull. 22 (1987) 631–639;
C. Delmas, A. Nadiri, J.L. Soubeyroux, Solid State Ionics 28–30 (1988) 419–423.
[11] K. Yoshida, K. Toda, K. Uematsu, M. Sato, Key Eng. Mater. 157–158 (1999) 289–296.
[12] J. Gaubicher, C. Wurm, G. Goward, C. Masquelier, L. Nazar, Chem. Mater. 12 (2000) 3240–3242.
[13] M. Morcrette, C. Wurm, C. Masquelier, in: Proceedings of the 1st Lithium Battery Discussions, Arcachon, France, 27–30 May 2001.
[14] J. Barker, M.Y. Saidi, US Patent 6,203,946 (2001).
[15] M. Sato, H. Ohkawa, K. Yoshida, M. Saito, K. Uematsu, K. Toda, Solid State Ionics 135 (2000) 137–142.
[16] M.Y. Saïdi, J. Barker, H. Huang, J.L. Swoyer, G. Adamson, Electrochem. Solid State Lett. 7 (7) (2002) A149–A151.
[17] L. Nazar, H. Huang, S.-C. Yin, T. Kerr, in: Proceedings of the 11th International Meeting on Lithium Batteries, Monterey, CA, 2002.
[18] S.C. Yin, H. Grondey, P. Strobel, H. Huang, L.F. Nazar, J. Am. Chem. Soc. 125 (2003) 326–327.
[19] H. Huang, S.C. Yin, T. Kerr, N. Taylor, L.F. Nazar, Adv. Mater. 14 (21) (2002) 1525–1528.
[20] C. Wurm, M. Morcrette, G. Rousse, L. Dupont, C. Masquelier, Chem. Mater. 14 (2002) 2701–2710.
[21] H.M. Rietveld, J. Appl. Crystallogr. 2 (1969) 65.
[22] J. Rodriguez-Carvajal, Phys. B 192 (1993) 55.
[23] A.B. Bykov, A.P. Chirkin, L.N. Demyanets, S.N. Doronin, E.A. Genkina, A.K. Ivanov-shits, I.P. Kondratyuf, B.A. Maksimov, O.K. Mel'nikov, L.N. Muradyan, V.I. Simonov, V.A. Timofeeva, Solid State Ionics 38 (1990) 31–52.
[24] M. Morcrette, C. Wurm, C. Masquelier, Solid State Sci. 4 (2002) 239–246.
[25] P.C. Christidis, P.J. Rentzeperis, Z. Kristallogr. 141 (1975) 233–245.
[26] W.H. Zachariasen, Acta Cryst. 16 (1963) 385–389.
[27] N.E. Brese, M. O'Keeffe, Acta Cryst. B47 (1991) 192–197.
[28] M. Morcrette, S. Patoux, C. Wurm, C. Masquelier, ECS Lett., in press.
[29] A. Manthiram, J.B. Goodenough, J. Power Sources 26 (1989) 403–408.
[30] C. Wurm, Thèse de Doctorat, Université Paris-XI Orsay, 12 July 2002.
[31] M. Sato, S. Tajimi, H. Okawa, K. Uematsu, K. Toda, Solid State Ionics, in press.
[32] K.S. Nanjundaswamy, A.K. Padhi, J.B. Goodenough, S. Okada, H. Ohtsuka, H. Arai, J. Yamaki, Solid State Ionics 92 (1996) 1–10.
[33] M. Sato, H. Ohkawa, K. Yoshida, M. Saito, K. Uematsu, K. Toda, Solid State Ionics 135 (2000) 137–142.
[34] J. Gopalakrishnan, K.K. Rangan, Chem. Mater. 4 (1992) 747–749.